

N O T I C E

THIS DOCUMENT HAS BEEN REPRODUCED FROM
MICROFICHE. ALTHOUGH IT IS RECOGNIZED THAT
CERTAIN PORTIONS ARE ILLEGIBLE, IT IS BEING RELEASED
IN THE INTEREST OF MAKING AVAILABLE AS MUCH
INFORMATION AS POSSIBLE

NOTICES PAGE

Foreign Nation Release

This information is furnished upon the condition that it will not be released to another Nation without specific authority of the cognizant agency (Military or NASA) of the United States Government, and that the information be provided substantially the same degree of protection afforded it by the Department of Defense of the United States.

Disclaimer of Liability from Act of Transmittal

When Government drawings, specifications, or other data are used for any purpose other than in connection with a definitely related Government procurement operation, the United States Government thereby incurs no responsibility nor any obligation whatsoever; and the fact that the Government may have formulated, furnished, or in any way supplied the said drawings, specification, or other data, is not to be regarded by implication or otherwise as in any manner licensing the holder or any other person or corporation, or conveying and rights or permission to manufacture, use, or sell any patented invention that may in any be related thereto.

Any information disseminated by the Data Distribution Centers of the Interagency Data Exchange Program is intended to promote test data utilization in the National interest among groups engaged in Ballistic Missile, Space Vehicle and related programs.

Dissemination of said information does not imply verification or endorsement of the information. The originator, in submitting the material is acting in accordance with the requirements of his contract, and neither the originator nor the disseminator assumes any liability to parties adopting any product, process or practice based upon the usage of the information. Its presenting the success or failure of one (or several) part number(s), model(s), lot(s) under specific environment and output requirements, does not imply that other products not herein reported on are either inferior or superior.

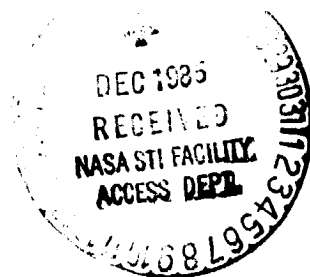
Omission of Charges for Follow-on Actions

Any compliance by the report originator with requests from recipients for more detailed information on IDEP reports originated under Government contracts will be considered within the scope of present contractual obligations. Compliance with such requests will be at the discretion of the report originator and will be performed without cost or obligation to the requestor unless otherwise negotiated in advance.

Reproduction of this Report

Reproduction or duplication of any portion of this report is expressly forbidden, except by those contractors receiving it directly from the Data Centers or originator, for their internal use or the use of their sub-contractors. Reproduction or display of all or any portion of this material for any sales, advertising or publicity purposes is prohibited.

December 12, 1985



Annual Technical Report for Grant No. NAGW-661

Covering the period from December 1, 1984 to November 30, 1985

Measurements of HO₂ Chemical Kinetics with a New Detection Method

Submitted by:

Long C. Lee, Masako Suto, and E. R. Manzanares
Department of Electrical & Computer Engineering
San Diego State University
San Diego, CA 92182
Tel. (619) 265-3701

Prepared for:

National Aeronautics and Space Administration
NASA Headquarters
Washington, D. C. 20546
Attention: Dr. R. F. Hampson
Upper Atmosphere Research Program, Code EE

N86-14789

(NASA-CR-176417) MEASUREMENTS OF HO₂
CHEMICAL KINETICS WITH A NEW DETECTION
METHOD Annual Technical Report, 1 Dec.
1984 - 30 Nov. 1985 (San Diego State Univ.,
Calif.) 39 p HC A03/MR A01 CSCL 04A G3/46

Unclas
05017

TABLE OF CONTENTS

I.	Introduction.....	3
II.	Research Accomplished.....	3
	A. Experimental Apparatus.....	3
	B. Production and Detection of HO ₂	5
	C. Reaction Rate Constant of HO ₂ + O ₃	5
	D. Photoexcitation Process of Cl ₂	9
III.	Cumulative Publications and Presentations.....	12
IV.	Appendix.....	13
	"Quantitative VUV Spectroscopy of Cl ₂ "	

I. INTRODUCTION

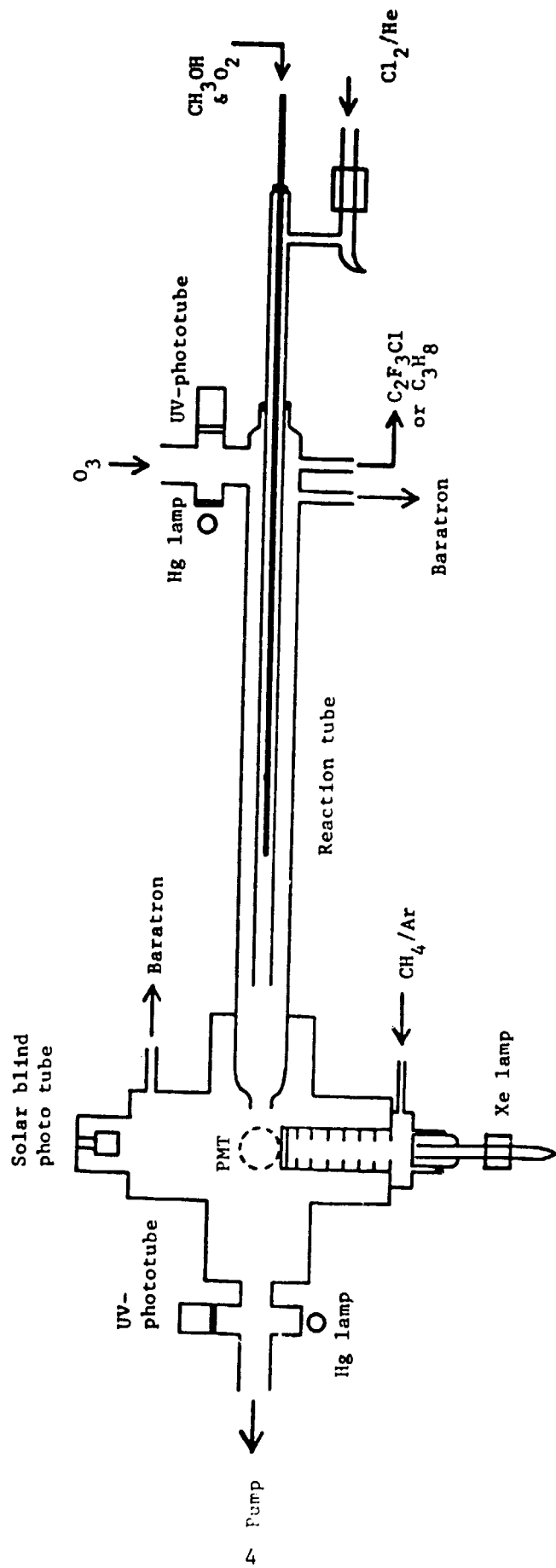
This report describes the results obtained in the period from December 1, 1984 to November 30, 1985 for the research program currently supported by NASA under Grant No. NAGW-661 basic. In this research program, HO₂ was detected by the OH(A-X) photofragment from dissociative excitation of HO₂ at 147 nm. This detection method was applied to measure the reaction rate constant of HO₂ + O₃. This reaction rate constant is needed for the understanding of stratospheric chemistry.

Since Cl₂ was used in the flow system, photoexcitation of Cl₂ may produce fluorescence to interfere with our measurements. Thus, the photoexcitation process of Cl₂ in the vacuum ultraviolet region was also examined in this research period using synchrotron radiation as a light source. The research results are summarized below.

II. RESEARCH ACCOMPLISHED

A. Experimental Apparatus

A discharge-flow-tube apparatus has been constructed in the current funding period. The schematic diagram for the apparatus is shown in Fig. 1. The flow tube consists of a large tube of 4.8 cm ID and 60 cm long, and a movable injector of 1 cm ID and 70 cm long. (The large tube of 4.8 ID was later changed to 2.3 cm to check the effect of walls on the reaction rate measurement). Inside the injector there is a small teflon tube of 2 mm ID. O₃ was produced by a high voltage a.c. discharge of O₂ and stored in two silica gel traps attached to the flow tube.



Experimental Setup

Fig. 1

The O₃ concentrations were monitored at two positions before and after the flow tube. HO₂ in a gas cell was detected by a Xe resonance light at 147 nm. The gas cell was a six-way cross of 3" OD which was made of stainless steel.

B. Production and Detection of HO₂

HO₂ was produced by microwave discharge of a trace of Cl₂ in He, which then reacted with CH₃OH and O₂ by



The measurements of gas pressures and the control of gas flow rates has been described in detail in the Semiannual Report.

HO₂ was detected by the OH(A-X) emission produced from photodissociative excitation of HO₂ by a Xe resonance light at 147 nm,



The attenuation of the light source and the quenching of OH*(A) by the gases in the gas cell were carefully examined, which were described in detail in the Semiannual Report.

C. Reaction Rate Constant of HO₂ + O₃

The reaction rate constant of HO₂ + O₃ has been measured by Zahniser and Howard [J. Chem. Phys. 73, 1620 (1980)] to be 2x10⁻¹⁵ cm³/s,

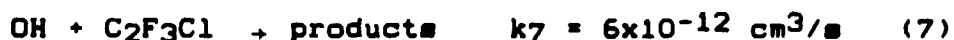


OH will react with O₃ to form HO₂ again,



with a reaction rate constant of 6.5x10⁻¹⁴ cm³/s. In order to measure the rate constant of reaction (5), the OH radicals need

to be scavenged. C_2F_3Cl and C_3H_8 were used as the OH scavengers in our experiments,



For $[O_3]$ varied in the 30-100 mtorr range in our experiments, 100 mtorr of C_2F_3Cl or 200 mtorr of C_3H_8 will effectively eliminate OH in the system. Thus, the effect of OH on the $HO_2 + O_3$ reaction rate measurement is minimized.

At each $[O_3]$, the pseudo-first-order-decay rate, K , of HO_2 was measured by the relative HO_2 concentration in the gas cell as a function of the $HO_2 + O_3$ reaction time by changing the HO_2 flow distance in the flow tube. The K values measured at various $[O_3]$ are shown in Fig. 2, where (200-250) mtorr of C_3H_8 was used as the OH scavenger. The reaction rate constant determined from the plot is $(2.1 \pm 0.5) \times 10^{-15} \text{ cm}^3/\text{s}$. This result is consistent with the value of Zahniser and Howard of $2.0 \times 10^{-15} \text{ cm}^3/\text{s}$.

We also measured the $HO_2 + O_3$ reaction rate constant using C_2F_3Cl as the OH scavenger. This molecule has been used by Zahniser and Howard in their $HO_2 + O_3$ kinetics measurements. The pseudo-first-order-decay rates of HO_2 as a function of $[O_3]$ are shown in Fig. 3, where about 120 mtorr of C_2F_3Cl was used as the OH scavenger. The reaction rate constant determined from the plot is $(1.5 \pm 0.4) \times 10^{-15} \text{ cm}^3/\text{s}$. In this measurement, we observed that C_2F_3Cl produced fluorescence in the UV region when it was excited by the 147 nm light. Although the fluorescence intensity was relatively small when a narrow band filter ($310 \pm 10 \text{ nm}$) was used to isolate the emission band, the fluorescence may somewhat

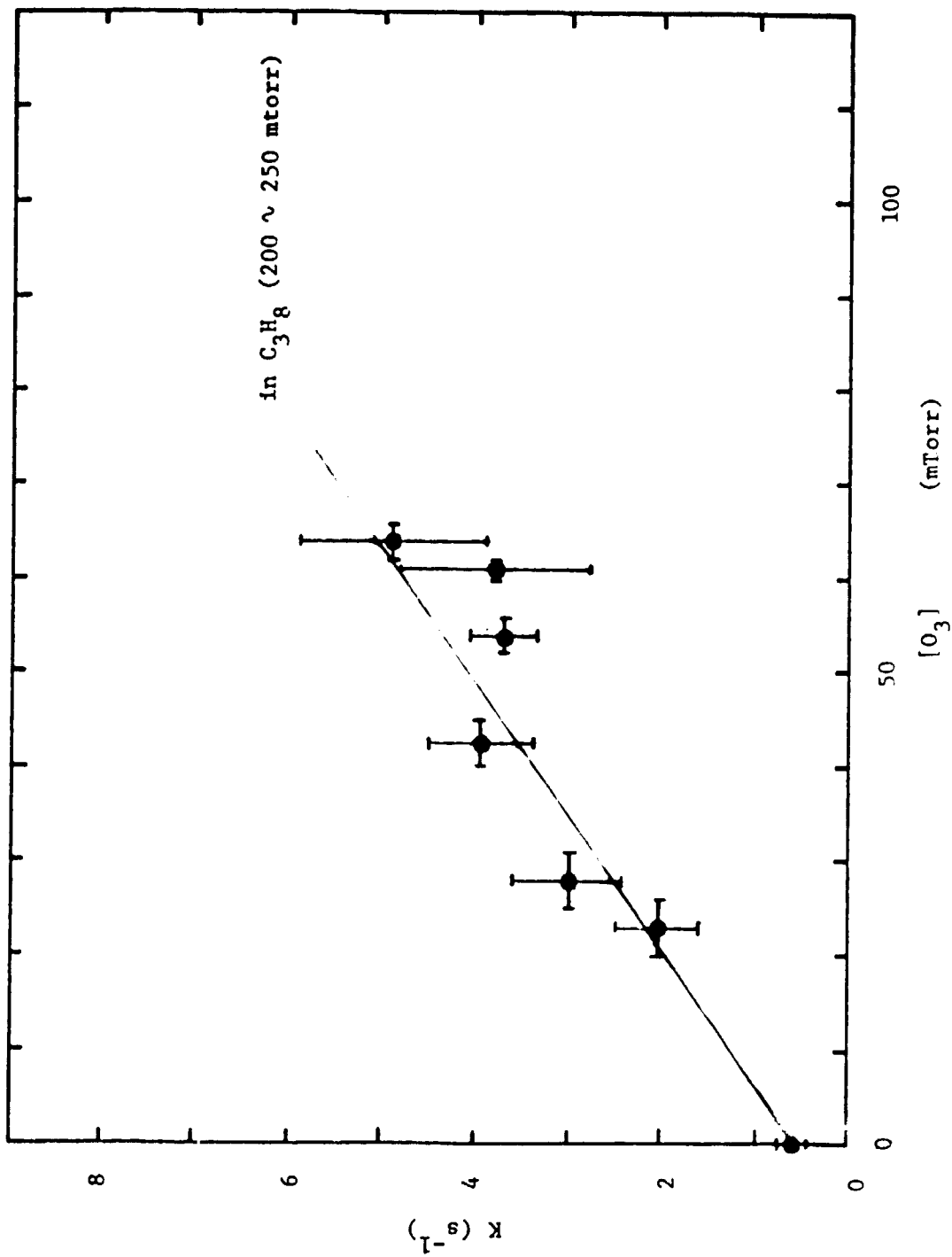


Fig. 2

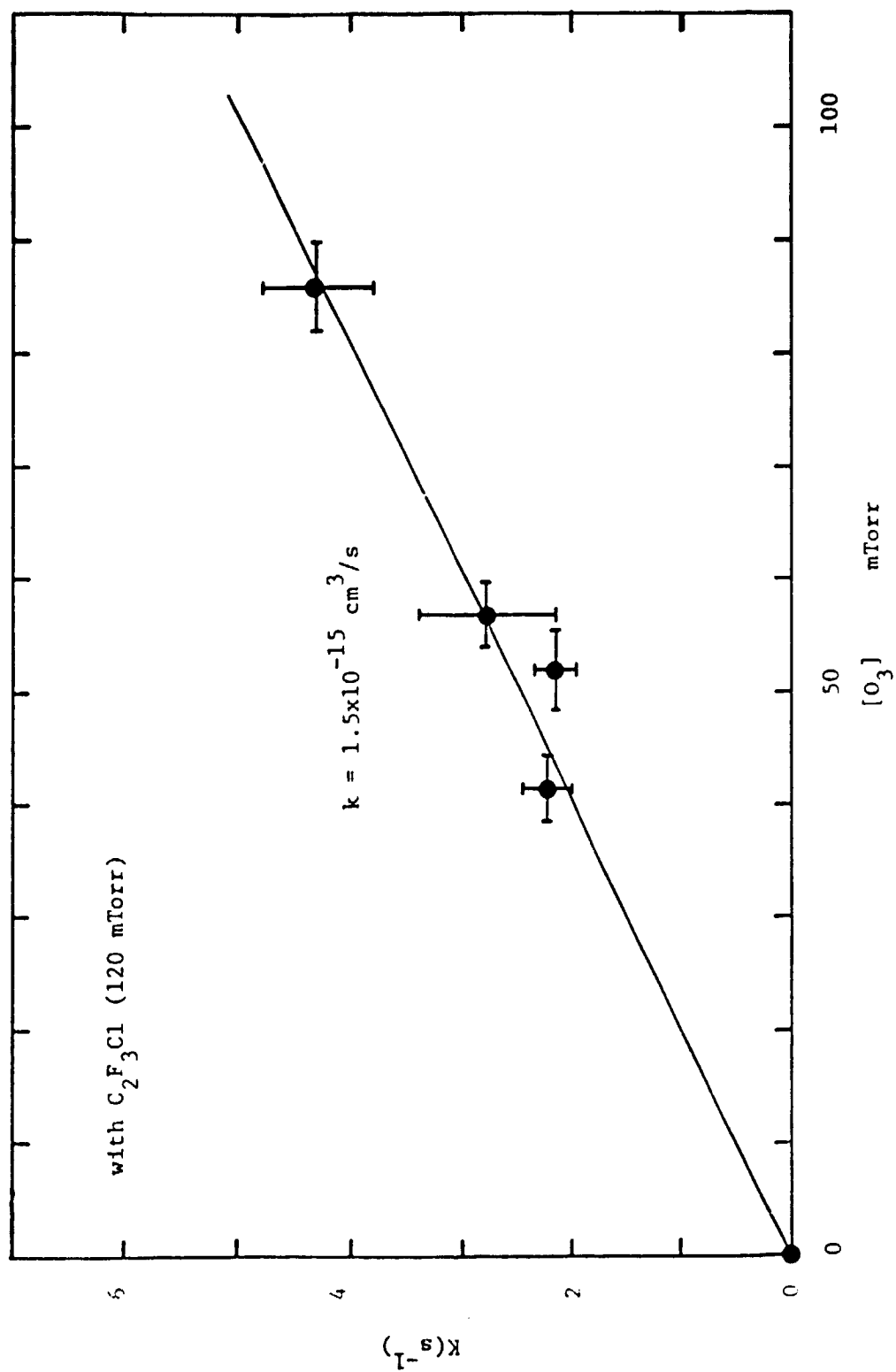


Fig. 3

disturb the observed signal. The fluorescence intensity from C_2F_3Cl has been corrected in the decay rate measurement.

In order to check the effect of walls on the measured reaction rate constant, we changed the flow tube size from 4.8 cm ID to 2.3 cm ID. The pseudo-first-order-decay rates of HO_2 measured with this small flow tube as a function of $[O_3]$ are shown in Fig. 4, where C_2F_3Cl was used as the OH scavenger. The reaction rate constant determined from the plot is $(1.7 \pm 0.2) \times 10^{-15} \text{ cm}^3/\text{s}$. This result will be checked again using C_3H_8 as the OH scavenger.

From the above results, the rate constant of the $HO_2 + O_3$ reaction (averaged over the data points) is $(1.8 \pm 0.3) \times 10^{-15} \text{ cm}^3/\text{s}$. We will take more data to reduce the experimental uncertainty, and then report the results in a scientific journal.

D. Photoexcitation Process of Cl_2

Cl_2 was used in the flow system to produce Cl atom that finally made HO_2 . We observed that Cl_2 has a weak ultraviolet fluorescence when excited at 147 nm. It is interesting to study the fluorescence process, because it is useful to assess the interference of the Cl_2 fluorescence to our kinetics measurements. In addition, the photodissociation process of Cl_2 is also of interest in the study of the upper atmospheric photochemistry. The photodissociation of Cl_2 by vacuum ultraviolet radiation in the upper atmosphere is a source of Cl atom. Based on these needs, we studied the photoexcitation process of Cl_2 using synchrotron radiation in the 105-200 nm region. The results are summarized in a paper entitled "Quantitative VUV Spectroscopy of Cl_2 " which is attached as an

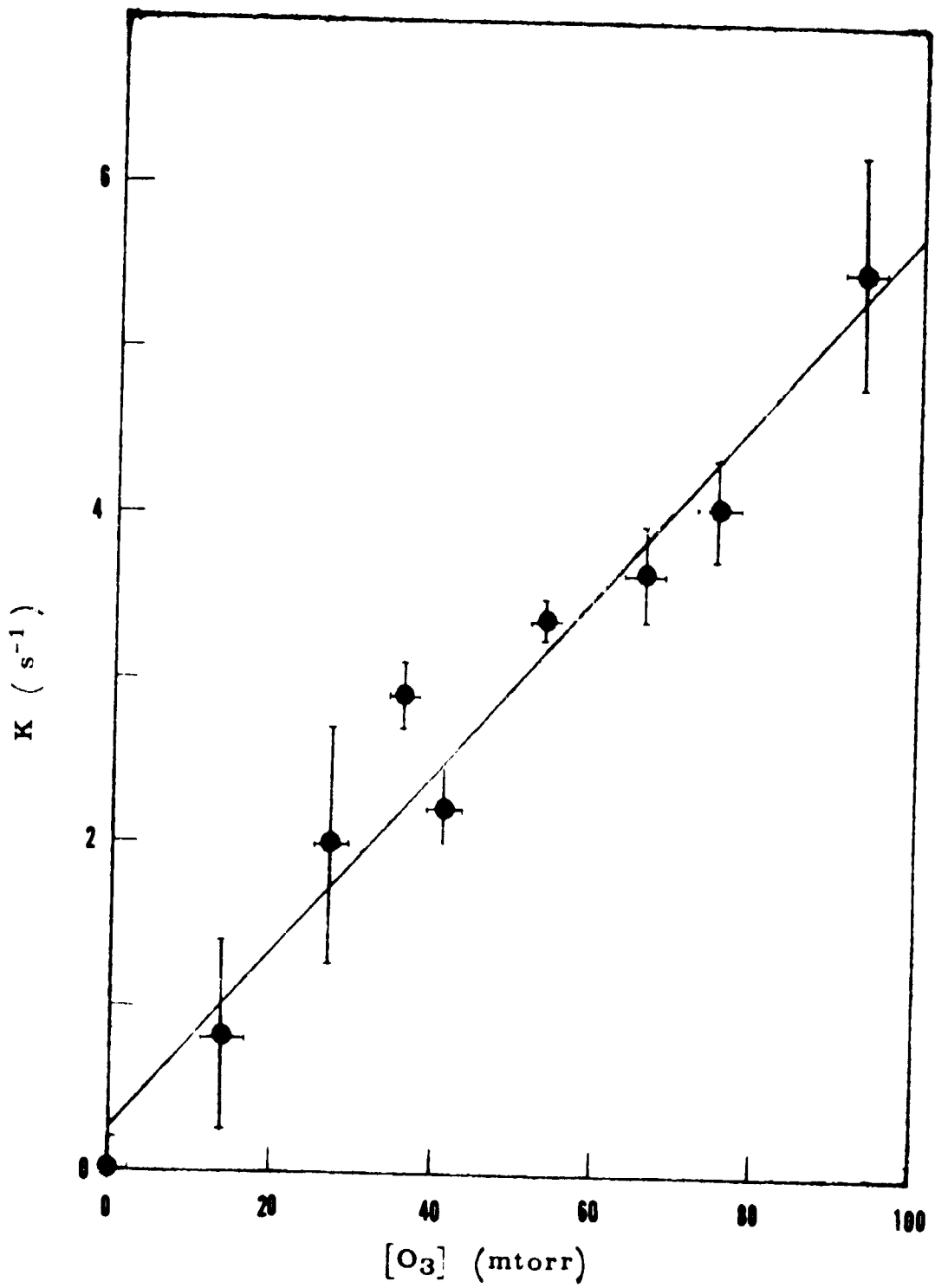


Fig. 4

Appendix. This paper has been submitted to the Journal of Chemical Physics for publication.

The absorption of Cl₂ in the VUV region is dominated by strong discrete structures. 147 nm is at the tail of the absorption band of the 1¹Σ⁺ Rydberg state. Both absorption and fluorescence cross sections of Cl₂ at 147 nm are quite small, thus, the fluorescence does not impose a serious interference to our kinetics measurements. The minor effect caused by the fluorescence from the photoexcitation of Cl₂ was corrected in the data shown in Figs. 2-4.

III. CUMULATIVE PUBLICATIONS AND PRESENTATIONS

Our preliminary works have been reported in scientific community as listed below:

1. M. Suto and L. C. Lee, "Photofragment Emission from HO₂ and its Application to the HO₂ Kinetics Study", presented at the Informal Atmospheric Kinetics Meeting, Jet Propulsion Laboratory, Pasadena, CA, Jan. 18, 1985.
2. M. Suto, "Study of the HO₂ + O₃ Reaction by Detecting HO₂ from Photofragment Emission", Seminar presented to the Naval Research Laboratory, Washington D. C., June 14, 1985.
3. L. C. Lee and M. Suto, "Photoexcitation Process of Cl₂ in VUV", presented at the 1985 SRC Users Group Meeting, Madison, Wisconsin, Oct. 21-22, 1985.
4. L. C. Lee, M. Suto and K. Y. Tang, "Quantitative VUV Spectroscopy of Cl₂", submitted to J. Chem. Phys. (1985).

IV. APPENDIX

"Quantitative VUV Spectroscopy of Cl₂"

Quantitative VUV Spectroscopy of Cl₂

L. C. Lee and Masako Suto
Department of Electrical and Computer Engineering
San Diego State University
San Diego, CA 92182

and

K. Y. Tang
Western Research Cooperation
9555 Distribution Ave.
San Diego, CA 92121

ABSTRACT

The photoabsorption and fluorescence cross sections of Cl₂ were measured in the 105-145 nm region using synchrotron radiation as a light source. The oscillator strengths for the major absorption bands are calculated from the measured absorption cross sections. The measured oscillator strengths for the $2^3\Pi_u$ and $2^1\Pi_u + X^1\Sigma_g^+$ transitions agree quite well with the theoretical values. The absorption spectrum was analyzed in accord with the excited electronic states calculated by Peyerimhoff and Buenker (1981). The Rydberg series converging to the first and second ionization potentials were classified. The vibrational levels of the $2^1\Sigma_u^+$ ionic state were determined up to $v' = 15$ from the fluorescence excitation spectrum. It was observed that a band with peak at 108.3 nm produces VUV fluorescence, but it produces UV fluorescence only by a collisional excitation process.

I. INTRODUCTION

The electronic transitions of chlorine molecule in the vacuum ultraviolet (VUV) region have been subject to extensive investigations.¹⁻⁴ Lee and Walsh¹ observed the absorption spectrum in the 107-210 nm region with a 1-m vacuum spectrograph. The absorption bands for wavelengths longer than 130 nm were assigned to possible electronic states in accord with molecular-orbital theory. However, the absorption bands at wavelengths shorter than 130 nm were so complicated that they were not analyzed. Iczkowski et al.² revisited the absorption spectrum in the 110-135 nm region in order to clarify the possible impurity (HCl) contamination of the Cl₂ spectrum observed by Lee and Walsh¹. A Rydberg series converging to the first ionization potential at 11.47 eV was found.²

The rotationally resolved absorption spectrum was observed and analyzed in the 133-145 nm region by Douglas³ using a 10.7 m vacuum spectrograph. An ionic state, $1^1\Sigma_u^+$, was determined from the analysis. The absorption spectrum in the 107-130 nm region has been taken by Douglas but it was not analyzed because of complexity. Recently, Moeller et al.⁴ studied the absorption spectrum of Cl₂ in the 120-140 nm region using synchrotron radiation. Fluorescence from the $1^1\Sigma_u^+$ state was observed and dispersed. The absorption spectrum was interpreted with the potential curves calculated by Peyerimhoff and Buenker⁵. The nature of the electronic transition of the absorption spectrum in the 130-145 nm region is now well understood,¹⁻⁵ although the transitions in the 105-130 nm region are still not clear.

The absolute absorption and fluorescence cross sections of Cl₂ in the VUV region are reported in this paper. These data are useful for understanding the nature of electronic states in the short wavelength region. The quantitative data are also needed in several application areas. For example, Cl₂ has been used in our laboratory for the study of HO₂ kinetics.⁶ The fluorescence cross section of Cl₂ is needed for examining the effect of Cl₂ fluorescence on the kinetics measurement. Cl₂ is also generally used in the chemical etching of semiconductor materials and in the rare gas-excimer laser. The quantitative photoexcitation data of Cl₂ are useful for understanding the role it plays in various environments. In addition to these practical applications, the oscillator strengths determined from the measured absorption cross sections are useful for comparison with the results of ab initio calculations.⁷

II. EXPERIMENTAL

The experimental set-up for the current measurement has been described in a previous paper.⁸ In brief, synchrotron radiation produced from the electron storage ring at the University of Wisconsin was dispersed by a 1-m Seya vacuum monochromator. The optical path of the absorption cell was 39.2 cm. The VUV light source was converted into UV light by sodium salicylate coated outside a LiF window and then detected by a photomultiplier tube (PMT). The fluorescence was monitored by a PMT (EMI 9558QB) in the UV-visible region and a solar blind PMT (EMI, CsI cathode) in the VUV region. The UV and VUV fluorescences were observed in directions orthogonal to the light beam. The UV fluorescence

cross section was calibrated by comparing the Cl₂ fluorescence intensity with the OH(A-X) fluorescence from photodissociation of H₂O, for which the fluorescence cross section is known.⁸ The fluorescence quantum yield is then determined from the ratio of fluorescence cross section to absorption cross section. The absolute cross section for the production of VUV fluorescence was calibrated by comparing the observed Cl₂ fluorescence intensity with the CO resonance fluorescence intensity, for which the CO fluorescence cross section is assumed to be equal to the CO absorption cross section.

Nature Cl₂ was supplied by Matheson with a stated purity of better than 99.9%, which was used in this experiment as delivered. The gas pressure was measured by a MKS Baratron capacitance manometer. The light source intensity, the gas pressure, and the fluorescence intensities were simultaneously monitored and analyzed by an IBM microcomputer.

III. RESULTS AND DISCUSSION

A. Photoabsorption Cross Section

The photoabsorption cross section of Cl₂ in the 105-145 nm region is shown in Fig. 1 for a monochromator resolution set at 0.1 nm. The cross section was derived from the light attenuation under the condition that the absorbance increases linearly with increasing Cl₂ pressure. The pressure range used in the absorption measurement depends on the absorption cross section, that is, the higher the absorption cross section, the smaller is the pressure range.

As shown in Fig. 1, the absorption spectrum is dominated by

sharp discrete structures. Thus, the measured cross section depends on the monochromator resolution. The apparent absorption cross section given in Fig. 1 represents the average value over the 0.1 nm bandwidth. The uncertainty is estimated to be $\pm 10\%$ of the given value. The wavelengths given by the high resolution spectra of Douglas³ and Moeller et al.⁴ were used as the wavelength reference in this experiment.

In contrast to the absorption cross section, the oscillator strength does not depend on the resolution. The oscillator strength can be determined⁹ from the measured average absorption cross section by

$$f = 11.3 \int \sigma(\lambda) d\lambda / \lambda^2$$

where $\sigma(\lambda)$ is the absorption cross section in unit of Mb (10^{-18} cm^2) and λ is the wavelength in unit of nm. The oscillator strengths for the strong absorption bands are listed in Table I. The experimental uncertainty is estimated to be $\pm 10\%$ of the given value.

The oscillator strengths for the $2^1\Pi_u$ and $2^3\Pi_u \leftarrow X^1\Sigma_g^+$ transitions have been recently calculated by Grein et al.⁷ whose values are 0.0699 and 0.0084, respectively. The sum of the measured oscillator strengths for the $2^1\Pi_u (v'=0-3) \leftarrow X^1\Sigma_g^+$ is 0.0635 as shown in Table I and Fig. 1. This measured value agrees very well with the calculated one. The oscillator strength for the $2^3\Pi_u (v'=0-3) \leftarrow X^1\Sigma_g^+$ transition determined from the data shown in Fig. 1 is 0.017. This value is larger than the calculated value by a factor of 2. However, depending on the energy difference between the $2^3\Pi_u$ and $2^1\Pi_u$ states the calculated value⁷ could be adjusted to 0.0122. This higher value agrees

reasonably well with our measurement. In considering both the experimental and theoretical uncertainties, the agreement is quite good.

The absorption bands are classified into Rydberg series, as shown in Fig. 1. The wavelengths, the wavenumbers, and the peak absorption cross sections for these Rydberg states are listed in Tables II-IV. The justification of the Rydberg state assignment is discussed below.

B. Rydberg States

The electronic configurations of Cl₂ have been studied by Lee and Walsh¹, for which the ground state, X¹Σ_g⁺, is given by



The potential curves of Cl₂ have been calculated by Peyerimhoff and Buenker⁵. The singlet states relevant to the interpretation of the observed strong transitions are shown in Fig. 2. Although the vertical excitation energies may need to be adjusted⁷, these potential curves are still good to serve the purpose of present discussion. The potential curves for most excited states are complicated by the perturbation of the ionic states such that they result in double wells.

The $1^1\Sigma_u^+$ ($\pi_g \rightarrow 4p\pi$) state is an ionic state which fluoresces. The vibrational levels of this ionic state were studied in great detail by Moeller et al.⁴, and the rotational spectra were analyzed by Douglas³. The fluorescence quantum yield for this state is close to 1 (see Discussion in the next section).

The $2^1\Pi_u$ state results from the $\pi_g \rightarrow 4p\sigma$ Rydberg transition.⁵ The effective quantum number of this Rydberg state

is $n^* = 2.46$ (a quantum defect of $\delta = 1.54$ for $n=4$), where the ionization potential¹⁰ of $92,590 \text{ cm}^{-1}$ (11.48 eV) was used for the calculation of n^* . Using this quantum defect, the Rydberg states with $n = 5$ and 6 are found as listed in Table II and also indicated in Fig. 1. The spin-orbital splitting for the first Cl_2^+ state, $X^2\Pi_{g1/2,3/2}$, is same as its vibrational frequency, thus, the photoelectron spectrum shows a single vibrational progression.^{11,12} The characteristics of the Rydberg states are usually the same as its converging ion state, that is the spin-orbital splitting for the $2^1\Pi_u$ and $3^1\Pi_u$ states are also similar to the vibrational frequency as shown in Fig. 1.

The vibrational levels of the $2^1\Sigma^+$ state were assigned by Moeller et al.⁴ The vibrational levels are now extended to $v'=15$ using the fluorescence excitation spectrum observed in the current experiment (see discussion in the next section). The $2^1\Sigma_u^+$ state results from the $\pi_g \rightarrow 4p\pi$ Rydberg transition⁵ (which may mix with the $\sigma_g \rightarrow \sigma_u$ transition) with an effective quantum number of $n^* = 2.75$ (a quantum defect of $\delta = 1.25$ for $n=4$). Using this quantum defect, the $n = 5$ and 6 Rydberg states are found as listed in Table III and also indicated in Fig. 1.

The absorption spectrum in the 105-115 nm region is complicated, and the transitions were not assigned before. According to the potential curves shown in Fig. 2, the absorption in this wavelength region likely corresponds to the $3^1\Pi_u \rightarrow X^1\Sigma_g^+$ transition. The calculated vertical excitation energy for this transition⁷ is 90501 cm^{-1} (110.50 nm). The $3^1\Pi_u$ state results

from the $\sigma_u + 4s$ Rydberg transition⁵, which converges to the second Cl_2^+ state, $A^2\Pi_1$. The vibrational levels of this ion state were observed to be a chaotic distribution.¹³ The vibrational levels were classified into five vibrational progressions, that is, system I (a), (b) and (c) and system II (d) and (e). Since the $3^1\Pi_u$ state is the Rydberg state converging to the $Cl_2^+(A)$ state, the vibrational spacings of these two states should be similar. This expectation is indeed true. The absorption structures in the 105-115 nm region are arranged into system I (a), (b) and (c) and system II (d) and (e) as shown in Fig. 1 in corresponding to the vibrational progressions of the $Cl_2^+(A)$ state. The wavelengths, vibrational frequencies, spacings, and peak cross sections for system I (a) and (b) are listed in Table IV. Both the chaotic distributions observed in the Rydberg and ion states indicate that the chaotic vibrational distribution occurs in nature. The other possibility¹³ that the chaotic vibrational distribution of the ion state is due to perturbation seems unlikely. The oscillator strengths for the system I (c) and system II (d) and (e) are relatively weak when compared with system I (a) and (b). The weaker systems may be due to the triplet state, $3^3\Pi_u$, similar to the case of $2^3\Pi_u$ mixed with $2^1\Pi_u$.

Taking the ionization potential^{11, 12, 14} of the $Cl_2^+(A)$ state at onset as 13.96 eV, the effective quantum number for the first vibrational level of system I(a) is $n^* = 2.10$ (the quantum defect $\delta = 1.90$ for $n=4$). Considering the quantum defect of $\delta = 1.54$ for the p-electron, this quantum defect of $\delta = 1.90$ for the s-electron is reasonable. This further supports the assignment of

the $3^1\Pi_u$ Rydberg state.

C. Fluorescence Cross Sections

The cross sections for the production of UV and VUV fluorescence measured at a monochromator resolution of 0.2 nm are shown in Fig. 3. The absorption cross section measured at the same resolution is also shown in Fig. 3 for comparison. The peak absorption cross section in Fig. 3(a) is generally smaller than that in Fig. 1, because the monochromator resolution used for Fig. 3(a) is lower.

The VUV fluorescence was detected by a solar blind PMT whose response was in the 115-180 nm region, and the UV fluorescence by a PMT (EMI 9558QB) in the 180-200 region (see the Experimental Section for the absolute calibration). The uncertainty for the UV fluorescence cross section is estimated to be $\pm 30\%$ of the given value, but for the VUV fluorescence the uncertainty can be a factor of 2.

The fluorescence from the $1^1\Sigma_u^+$ ionic state has been observed by several investigators,^{4,15,16} although the absolute fluorescence cross section was not reported before. The fluorescence excitation spectrum in the 130-140 nm region has been studied by Moeller et al.⁴ They also dispersed the fluorescence spectrum which covers from the excitation wavelength to 208 nm⁴. In our experiment, when an optical filter (transmitting wavelengths longer than 300 nm) was placed in front of PMT, the fluorescence disappeared. This confirms that the fluorescence spectrum is limited in the UV and VUV regions. The VUV fluorescence likely results from the $1^1\Sigma_u^+ \rightarrow X^1\Sigma_g^+$ transition,

and the UV fluorescence from the $1^1\Sigma_u^+ \rightarrow 1^1\Pi_g$ transition.

The VUV and UV fluorescence excitation spectra for the $1^1\Sigma_u^+$ state are generally the same as the absorption spectrum as shown in Fig. 3, except for the band at 136.2 nm where the VUV fluorescence is relatively more intense than the UV fluorescence. The cross section for the VUV fluorescence is larger than the UV fluorescence by a factor of about 5. At each wavelength in the 135-150 nm region, the sum of the VUV and UV fluorescence cross sections is about equal to the absorption cross section, indicating that the fluorescence quantum yield is nearly equal to 1. This result shows that the $1^1\Sigma_u^+$ state is not predissociative.

At low gas pressure, both the UV and VUV fluorescence intensities of the $1^1\Sigma_u^+$ state increase with increasing gas pressure as shown in Fig. 4(a), where the excitation wavelength is 135.2 nm. The fluorescence intensity does not increase further at high gas pressure. This saturation effect is due to the pre-absorption of light source intensity by the gas between the entrance and the PMT view region. The absorbance, which is defined as $\ln(I_0/I)$ for the light source intensities with (I) and without (I_0) Cl_2 in the gas cell, is also shown in Fig. 4(a) for comparison. The saturation of the absorbance at high gas pressure is due to total absorption of some rotational lines by the gas. For the absorption cross section measurement the pressure is limited to the region that the absorbance is linearly dependent on the gas pressure as mentioned before.

The fluorescence from the second ionic state, $2^1\Sigma_u^+$, is not well studied. We observe that this state fluoresces up to $v'=15$ as shown in Fig. 3(b). The wavelengths of the observed

vibrational levels are listed in Table II. This result demonstrates that the fluorescence excitation spectrum provides useful information to identify electronic states, which are otherwise difficult to be identified from the absorption spectrum because of overlapping of several electronic transitions. The fluorescence quantum yield for the $2^1\Sigma_0^+$ state is generally less than 1, indicating that this state is partially dissociative. This state may be heavily perturbed by the triplet states that do not fluoresce.

At wavelengths shorter than 109.7 nm, a VUV fluorescence band appears as shown in Fig. 3(b). At low gas pressure, the VUV fluorescence intensity increases linearly with gas pressure as shown in Fig. 4(b). At high gas pressure, the VUV fluorescence intensity is saturated due to pre-absorption. The VUV fluorescence is saturated at the gas pressure lower than that for the absorbance. This is caused by the fact that the VUV fluorescence is absorbed by the Cl_2 gas before it reaches the window of the solar blind PMT. Because of such difficulty as well as the spectral response being not corrected, the uncertainty for the absolute VUV fluorescence cross section in this excitation wavelength region is quite high (a factor of 2-3). Nevertheless, the fluorescence quantum yield for this excitation band is quite large. The excitation energy of this absorption band is higher than the ionization potential, thus, it is a so-called "superexcited state". The fluorescence yield for a "superexcited state" is usually small. The high fluorescence yield observed in this excitation band presents an interesting

case.

When the Cl_2 pressure increases, fluorescence in the UV region appears. The UV fluorescence intensity depends on the gas pressure quadratically as shown in Fig. 4(b), where the excitation wavelength is 108.25 nm. This result indicates that the UV fluorescence is not primarily produced by photoexcitation but by collisional-induced excitation. The UV fluorescence may result from energy transfer from excited species to Cl_2 , where the excited species are produced by photoexcitation. The cross section for the production of UV fluorescence by primary photoexcitation process is practically zero. The dashed curve shown in Fig. 3(c) is only an excitation spectrum, which does not represent the absolute fluorescence cross section for the primary photoexcitation process. It is noted that the UV fluorescence has a significant intensity at few mtorr. This indicates that the excited state has a sufficient long lifetime which could be longer than 20 μs as estimated from gas collision kinetics. This lifetime is much longer than the lifetime of the VUV radiative state that is expected to be in the ns region. This result indicates that the UV and VUV fluorescence are produced from different states.

The nature of the fluorescence band in the 106-110 nm region is not clear and it deserves to be studied more. The excitation spectra for both UV and VUV fluorescence at pressures 2.0, 4.9 and 11.1 mtorr are shown in Fig. 5. The intensity for the VUV fluorescence increases linearly with Cl_2 , but the UV fluorescence increases quadratically for the entire excitation band. The light source intensity in this wavelength region is nearly

constant, and it is not corrected in Fig. 5. It is noted that the excitation spectrum for the UV fluorescence is different from the VUV fluorescence, indicating that they are produced from different excited states as expected from the estimation of the different lifetimes. Similar structures appear at both the UV and VUV excitation spectra as well as repeatedly shown in the absorption spectrum.

The VUV fluorescence is not produced from the excited atomic chlorine, because the excitation photon energy is not enough to produce excited chlorine atoms. For instance, the dissociation energy¹⁷ of Cl₂ is 2.479 eV, the wavelength threshold for producing the Cl(2P-2P_{3/2}) emission of 134.7 nm is 106.1 nm. This threshold wavelength is shorter than the threshold of the fluorescence band that starts at 110 nm.

IV. CONCLUDING REMARKS

The photoabsorption and fluorescence cross sections of Cl₂ in the VUV region are measured using synchrotron radiation as a light source. The structures shown in the absorption spectrum are classified into Rydberg series. The structures shown in the photoabsorption spectrum are generally observed in the threshold-electron-impact excitation spectrum¹⁸ and the electron energy loss spectrum.¹⁹ The resolution for the current photoabsorption spectrum is much higher than the electron spectra,^{18,19} thus, the structures are much better resolved and assigned.

The Fluorescence yield for the $1^1\Sigma_u^+$ state is very high (close to 1). Thus, this fluorescence system can be used to

develop techniques for a remote sensing of Cl₂ in various environments, such as plasma etching vessel. In other case, the fluorescence cross section of Cl₂ at 147 nm is so small that the existence of Cl₂ in the flow tube does not affect the HO₂ kinetics measurement. The fluorescence excitation spectrum is also a useful tool for spectroscopic study. As an example, the vibrational levels of the 2¹Σ_u⁺ ionic state are observed up to v'=15 with the aid of fluorescence excitation spectrum. It is interesting that the absorption band in the 106-110 nm region has a large quantum yield to produce VUV fluorescence, but the yield for the UV fluorescence is essentially zero. The UV fluorescence is produced by a collisional excitation process. The nature of this excitation process is not understood and it will be interesting to pursue further.

ACKNOWLEDGEMENT

This research program is partly in cooperation with Dr. T. J. Chuang at IBM Laboratory, San Jose. We wish to thank Dr. C. S. Lee, Dr. E. R. Manzanara, Dr. J. B. Nee, and Dr. W. C. Wang in our laboratory for useful discussion. The authors are grateful to the staff of the Synchrotron Radiation Center of the University of Wisconsin. The SRC facility is supported by the NSF under Grant No. DMR-77-21888. This work is supported by the NSF under Grant No. CBT-8518555 and the NASA under Grant No. NAGW-661.

REFERENCES

1. J. Lee and A. D. Walsh, *Trans. Faraday Soc.* 55, 1281 (1959).
2. R. P. Iczkowski, J. L. Margrave and J. W. Green, *J. Chem. Phys.* 33, 1261 (1960).
3. A. E. Douglas, *Can. J. Phys.* 59, 835 (1981).
4. T. Moeller, B. Jordan, P. Gürtler, G. Zimmerer, D. Haaks, J. LeCalve, M. Castex, *Chem. Phys.* 76, 295 (1983); *idib.*, Spectral Line Shapes, Vol. 2, Ed. K. Burnett (Walter de Gruyter, Berlin, 1983), P. 597.
5. S. D. Peyerimhoff and R. J. Buenker, *Chem. Phys.* 57, 279 (1981).
6. W. C. Wang, M. Suto, and L. C. Lee, *J. Chem. Phys.* 81, 3122 (1984).
7. F. Grein, S. D. Peyerimhoff, and R. J. Buenker, *Can. J. Phys.* 62, 1928 (1984).
8. L. C. Lee, *J. Chem. Phys.* 72, 4334 (1980).
9. L. C. Lee and J. A. Guest, *J. Phys. B: At. Mol. Phys.* 14, 3415 (1981).
10. K. Watanabe, *J. Chem. Phys.* 26, 542 (1957).
11. A. W. Potts and W. C. Price, *Trans. Faraday Soc.* 67, 1242 (1971).

12. A. B. Cornford, D. C. Frost, C. A. McDowell, J. L. Ragle, and I. A. Stenhouse, *J. Chem. Phys.* 54, 2651 (1971).
13. F. P. Huberman, *J. Mol. Spectros.* 20, 29 (1966).
14. T. A. Carlson, M. O. Krause, F. A. Grimm, and T. A. Whitley, *J. Chem. Phys.* 78, 638 (1983).
15. Y. V. Rao and P. Venkateswarlu, *J. Mol. Spectrosc.* 9, 173 (1962).
16. A. E. Douglas and A. R. Hoy, *Can. J. Phys.* 53, 1965 (1975).
17. K. P. Huber and G. Herzberg, Constants of Diatomic Molecules, (Van Nostrand, New York, 1979).
18. J. Jureta, S. Cvejanović, M. Kurepa, and D. Cvejanović, *Z. Phys. A.* 304, 143 (1982).
19. D. Spence, R. H. Huebner, H. Tanaka, M. A. Dillon, and R. G. Wang, *J. Chem. Phys.* 80, 2989 (1984).

Table I

Integration of absorption cross section over wavelength, $\int \sigma d\lambda$, in units of Mb·nm and oscillator strength, f , in units of 10^{-3} for the major absorption bands.

wavelength (nm)	$\int \sigma(\lambda) d\lambda$ (Mb·nm)	$f(10^{-3})$
111.50-111.77	21.7	19.7
112.58-112.85	22.9	20.4
113.17-113.39	19.0	16.7
113.66-114.01	29.4	25.6
114.12-114.47	22.4	19.4
116.96-117.15	10.1	8.3
117.82-117.98	9.7	7.9
124.74-125.00	9.1	6.6
126.36-126.63	12.7	9.0
127.84-128.38	31.6	21.8
130.84-131.14	5.9	3.9
132.00-132.19	19.6	12.7
133.11-133.30	36.2	23.1
134.22-134.47	37.8	23.7
135.01-135.95	83.5	51.5
135.95-136.49	43.0	26.2

Table II

Effective quantum number, n^* , wavelength, $\lambda(\text{nm})$, wavenumber, $\nu(\text{cm}^{-1})$, vibrational spacing, $\Delta\nu(\text{cm}^{-1})$, and peak absorption cross section, $\sigma_p(\text{Mb})$, for the $\pi_g \rightarrow n p \sigma$ Rydberg Series.

n	n^*	v'	$\lambda(\text{nm})$	$\nu(\text{cm}^{-1})$	$\Delta\nu(\text{cm}^{-1})$	$\sigma_p(\text{Mb})$
4 ($2^1\Pi_u$)	2.46	0	134.33	74,443		301.5
		1	133.22	75,064	621	315.6
		2	132.10	75,700	636	157.6
		3	131.04	76,313	613	39.0
		4	130.14	76,840	527	
		5	129.22	77,387	547	
5	3.46	0	119.87	83,424		35.3
		1	119.02	84,019	595	42.9
		2	118.18	84,617	598	
6	4.41	0	115.02	86,941		
		1	114.40	87,413	472	
∞			108.00	92,590		

Table III
Spectroscopic data for the $\pi_g \rightarrow n\pi$ Rydberg Series

n	n^*	v'	$\lambda(\text{nm})$	$\nu(\text{cm}^{-1})$	$\Delta\nu(\text{cm}^{-1})$	$\sigma_p(\text{Mb})$
4 ($2^1 \Sigma_u^+$)	2.75	0	128.01	78,119		133.9
		1	126.45	79,083	964	84.3
		2	124.89	80,070	987	58.6
		3	123.66	80,867	797	28.2
		4	122.33	81,746	879	
		5	121.17	82,529	783	
		6 ^a	120.18	83,209	680	
		7	118.94	84,076	867	
		8	117.92	84,803	727	
		9	116.81	85,609	806	
		10	116.02	86,192	583	
		11	115.18	86,821	629	
		12	114.28	87,504	683	
		13	113.37	88,207	703	
		14	112.59	88,818	611	
15	111.81	89,437	619			
5	3.75	0	117.92	84,803		84.9
		1	117.08	85,412	609	94.9
		2	116.32	85,970	558	54.7
		3	115.50	86,580	610	
6	4.68	0	114.18	87,581		
∞			108.00	92,590		

a The wavelengths for the vibrational levels from $v'=6$ to 15 were determined from the fluorescence excitation spectra.

Table IV
Spectroscopic data for the $\pi_u \rightarrow 4s (3^1\Pi_u)$ Rydberg Transition

Vibrational Series		$\lambda(\text{nm})$	$\nu(\text{cm}^{-1})$	$\Delta\nu(\text{cm}^{-1})$	$\sigma_p(\text{Mb})$
I	a	113.91	87,789		143.1
		112.75	88,692	903	130.3
		111.65	89,566	874	101.5
		110.72	90,318	752	
		109.70	91,158	840	
		108.94	91,794	636	
		108.20	92,421	627	
		107.46	93,058	637	
		106.72	93,703	645	
	b	113.28	88,277		122.6
		112.06	89,238	961	
		110.98	90,106	868	
		110.02	90,893	787	
		109.25	91,533	640	
		108.49	92,174	641	
	107.75	92,807	633		
	107.03	93,432	625		

FIGURE CAPTIONS

- Fig. 1 Photoabsorption cross section of Cl₂ in the 105-145 nm region measured with 0.1 nm resolution. The wavelength positions for the Rydberg transitions are indicated.
- Fig. 2 The potential curves of the singlet states relevant to the discussion in this paper. These curves are adopted from Ref. 5.
- Fig. 3 (a) absorption, (b) VUV fluorescence, and (c) UV fluorescence cross sections measured with 0.2 nm resolution. The vibrational levels of the $2^1 \Sigma_u^+$ are indicated in (b). The dashed curve in (c) is an excitation spectrum which does not represent absolute value.
- Fig. 4 The pressure dependence of the absorbance, VUV and UV fluorescence intensities measured at (a) 135.20 nm and (b) 108.25 nm.
- Fig. 5 Dependence of excitation spectra of (a) VUV and (b) UV fluorescence on Cl₂ pressures of (1) 2.0, (2) 4.9, and (3) 11.1 mtorr.

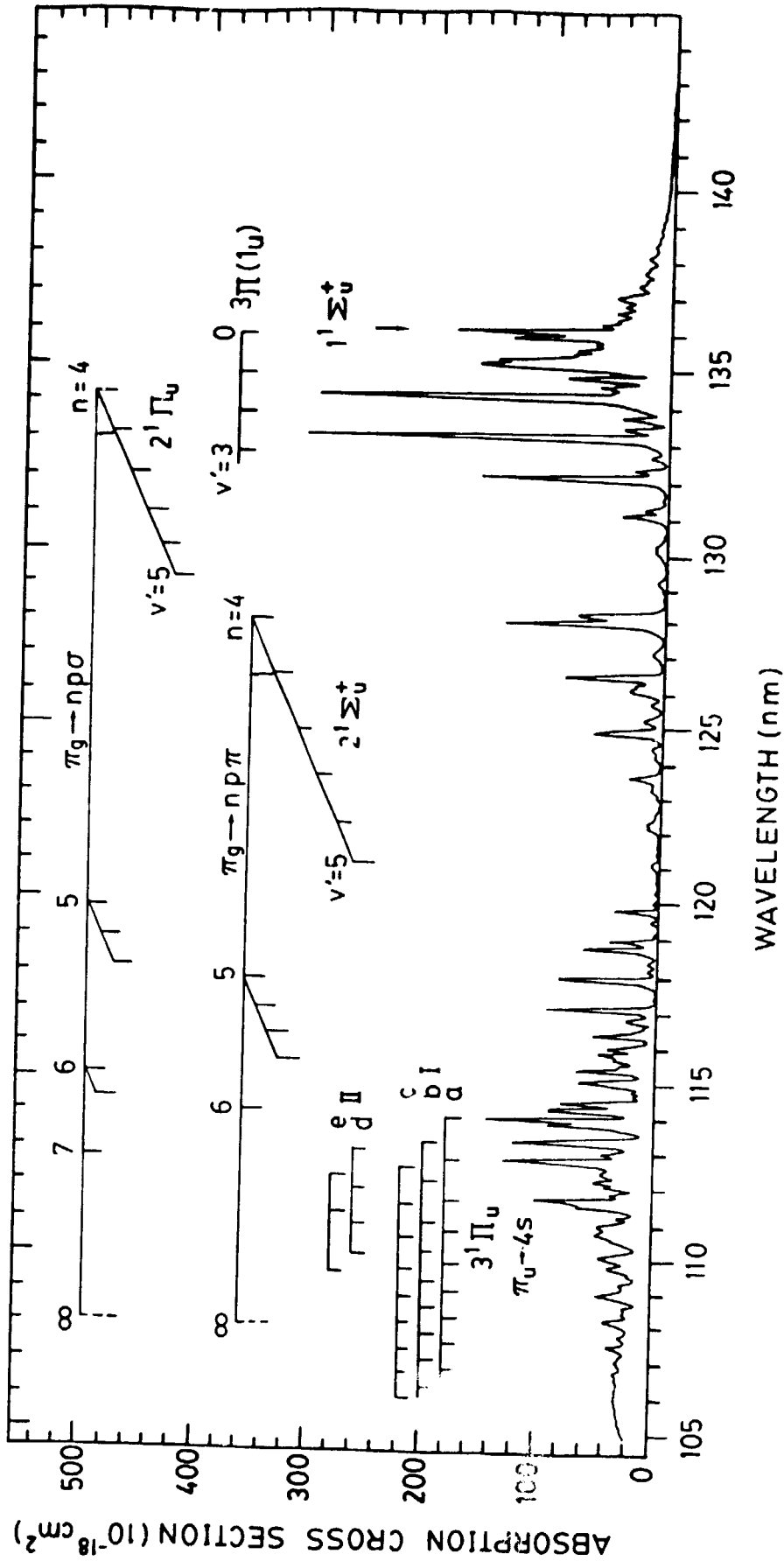


Fig 1

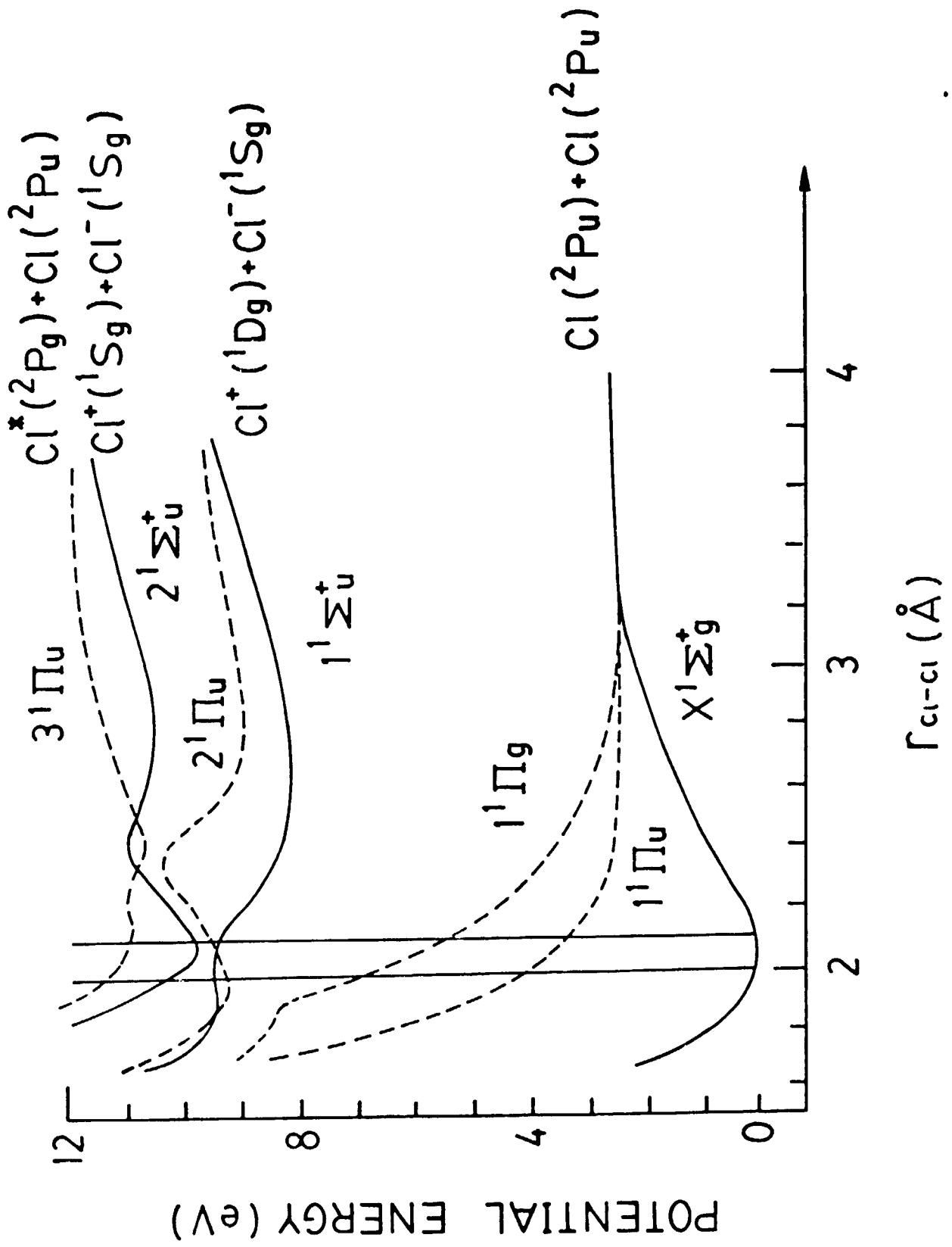


Fig. 2

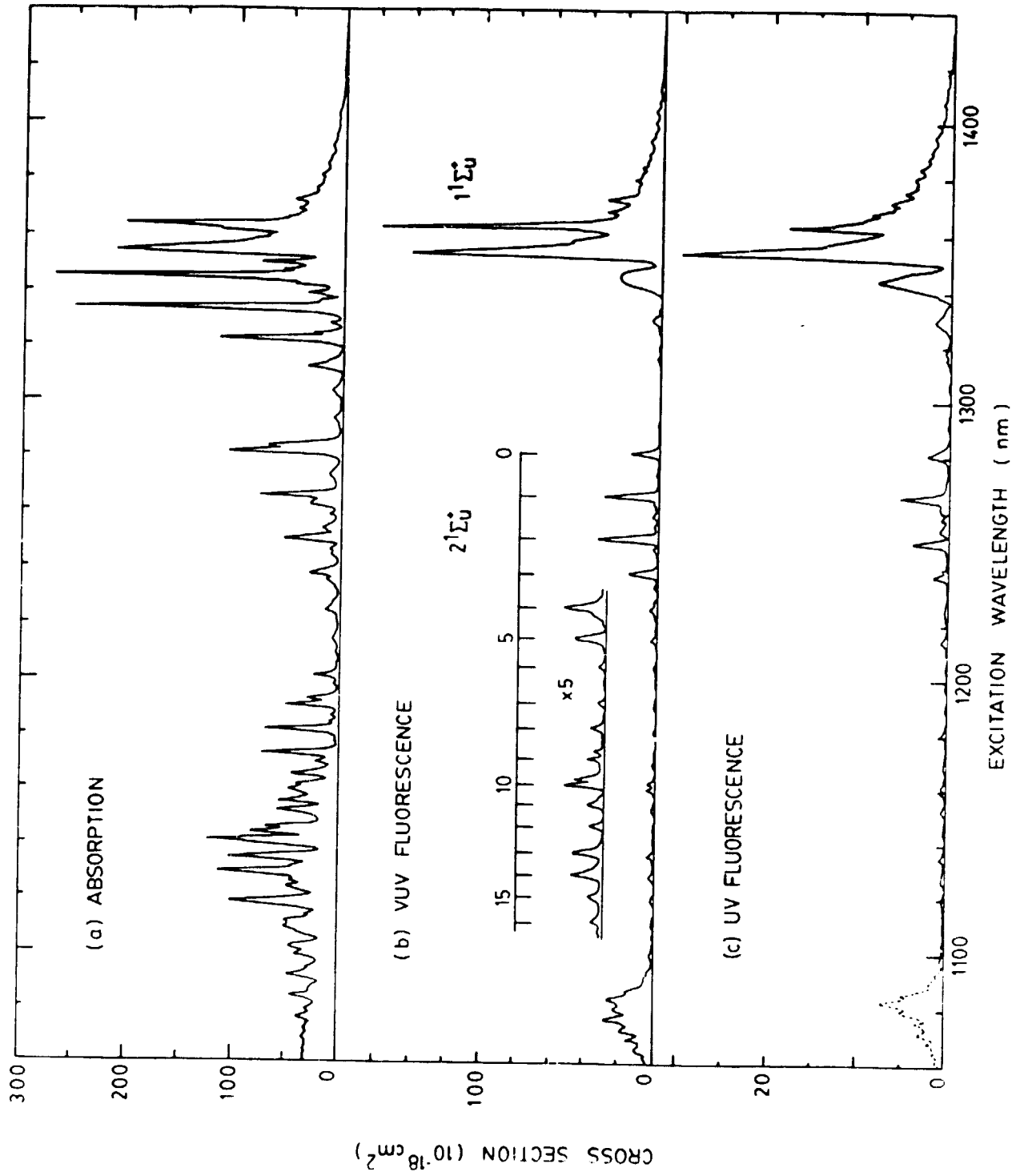


Fig. 3

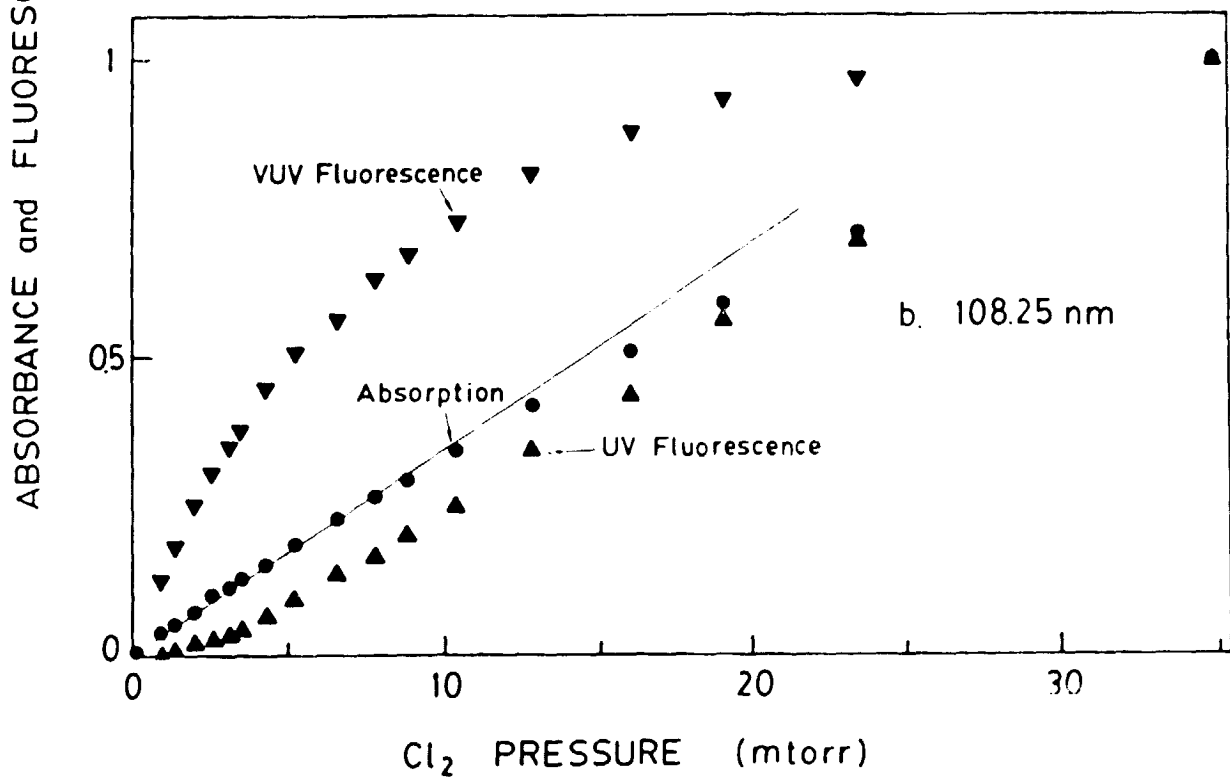
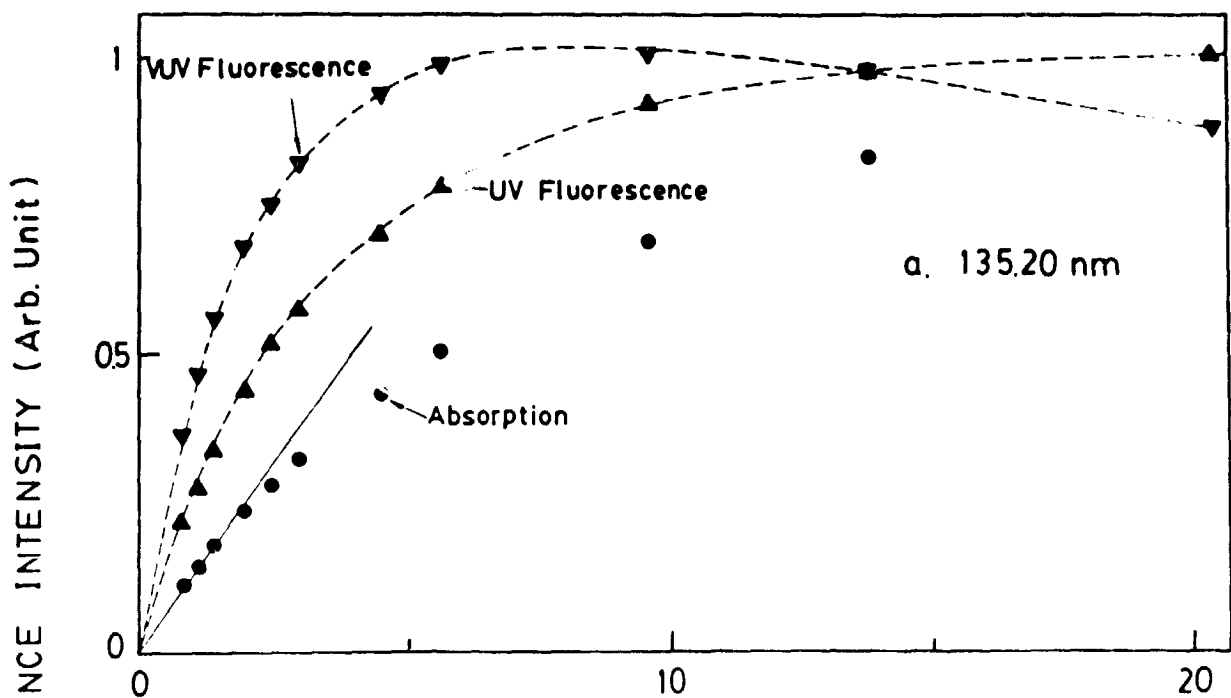


Fig. 4

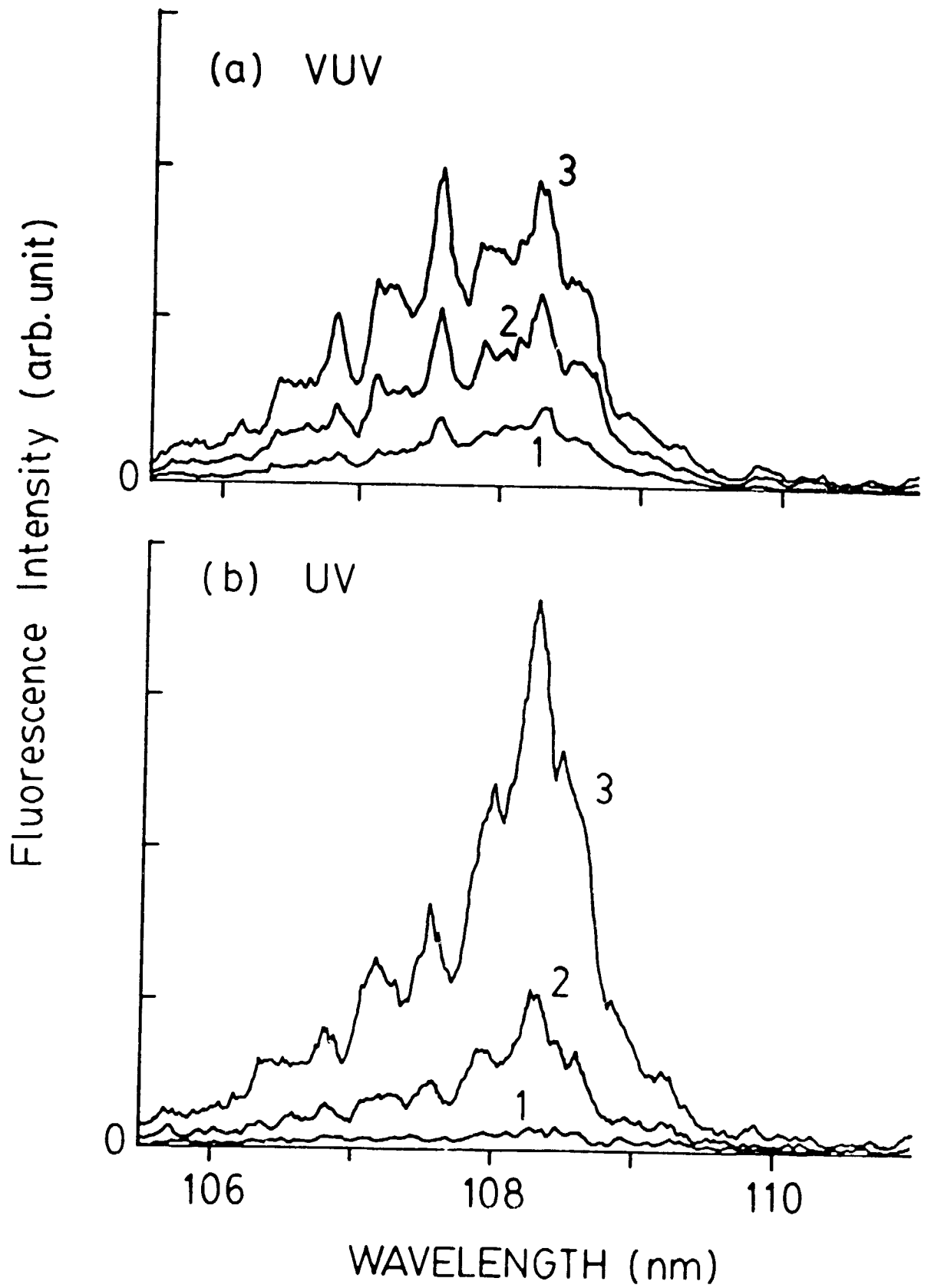


Fig. 5